

Burst-dependent plasticity and dendritic amplification support target-based learning and hierarchical imitation learning

Cristiano Capone*
INFN, Sezione di Roma, Rome, Italy
cristiano0capone@gmail.com

Cosimo Lupo*
INFN, Sezione di Roma, Rome, Italy

Paolo Muratore
SISSA, International School for
Advanced Studies, Trieste, Italy

Pier Stanislao Paolucci
INFN, Sezione di Roma, Rome, Italy

*These authors contributed equally to this work

Keyword: Target-based learning, Burst-dependent plasticity, hierarchical imitation learning

Abstract

The brain can learn to solve a wide range of tasks with high temporal and energetic efficiency. However, most biological models are composed of simple single compartment neurons and cannot achieve the state-of-art performances of artificial intelligence. We propose a multi-compartment model of pyramidal neuron, in which bursts and dendritic input segregation give the possibility to plausibly support a biological target-based learning. In target-based learning, the internal solution of a problem (a spatio temporal pattern of bursts in our case) is suggested to the network, bypassing the problems of error backpropagation and credit assignment. Finally, we show that this neuronal architecture naturally supports the orchestration of “hierarchical imitation learning”, enabling the decomposition of challenging long-horizon decision-making tasks into simpler subtasks.

1 Introduction

The brain can learn a wide range of tasks very efficiently in terms of energy consumption and required evidences, motivating the search for biologically inspired learning rules for improving the efficiency of artificial intelligence. Most biologically plausible neural networks are composed so far of point neurons. Despite recent outstanding advances in this field [Nicola and Clopath, 2017, Bellec et al., 2020], biologically plausible neural networks cannot achieve the state-of-art performances of artificial intelligence (e.g. they struggle to solve the credit assignment problem [Payeur et al., 2021]).

Recent findings on dendritic computational properties [Poirazi and Papoutsis, 2020] and on the complexity

of pyramidal neurons dynamics [Larkum, 2013] motivated the study of multi-compartment neuron model in the development of new biologically plausible learning rules [Urbanczik and Senn, 2014, Guerguiev et al., 2017, Sacramento et al., 2018, Payeur et al., 2021].

Recent works have proposed that segregation of dendritic input (neurons receive sensory information and higher-order feedback in segregated compartments) [Guerguiev et al., 2017] and generation of high-frequency bursts of spikes [Payeur et al., 2021] would support backpropagation in biological neurons. However, these approaches require propagating errors with a fine spatio-temporal structure to all the neurons. It is not clear whether this is possible in biological networks. For this reason, in the last few years, target-based approaches [Lee et al., 2015, DePasquale et al.,

2018, Manchev and Spratling, 2020, Meulemans et al., 2020, Muratore et al., 2021] started to gain more and more interest.

In a target-based learning framework, the targets, rather than the errors, are propagated through the network [Lee et al., 2015, Manchev and Spratling, 2020]. In this framework, it is possible to directly suggest to the network the internal solution to a task [DePasquale et al., 2018, Muratore et al., 2021, Capone et al., 2021]. However, target-based approaches require evaluating at the same time the spontaneous activity and the target activity of the network [DePasquale et al., 2018, Muratore et al., 2021]. This is usually solved by evaluating the two activities in two different networks, which is not natural in terms of biological plausibility.

In the present work, we show that bursts and dendritic input segregation offer a natural solution to this dilemma. In our model, pyramidal neurons rely on two different apical dendritic compartments to simultaneously evaluate the target and the spontaneous activity. A coincidence mechanism between basal and apical inputs generating the burst [Larkum, 2013] eventually defines the (target or spontaneous) spatio-temporal bursting dynamics of the network.

We exploit dendritic computation in our model, to let abstract signals act as teaching signals which drive the learning procedure in a biologically plausible fashion.

Finally, we show that this neuronal architecture naturally allows for orchestrating “hierarchical imitation learning”, enabling the decomposition of challenging long-horizon decision-making tasks into simpler subtasks [Le et al., 2018, Pateria et al., 2021].

2 Results

2.1 Target-based learning with bursts

We define a model of pyramidal neuron (Fig.1A, bottom) composed of three separated compartments, the basal one (i.e. the soma, receiving the sensorial input), and two apical ones, the proximal apical compartment (receiving recurrent connections from the network) and the distal apical compartment (receiving the context/teaching signal from other areas of the cortex, with a higher level of abstraction).

The spike emitted by the soma is described by variable z_i^t , which is equal to *one* when the spike is emitted at time t and *zero* otherwise. The spikes emitted by the proximal and distal apical compartments are described by the variables a_i^t and a_i^{*t} , respectively. The underlying idea is that the distal compartment

provides a target for the proximal one, motivating the use of the superscript symbol \star , which indicates the variables concerning the targets.

In addition, following [Larkum, 2013] a coincidence mechanism between the basal and the apical compartments has been implemented, yielding high-frequency bursts of spikes. In more detail, after a somatic spike, $z_i^t = 1$, a coincidence window is opened for a time interval ΔT . This is described by the variable \bar{z}_i^t , the indicator function for $t' \in [t, t + \Delta T]$, which is *one* during this time window. If a spike is generated by the distal or proximal apical compartments within such time window, $a_i^{t'} = 1$ or $a_i^{*t'} = 1$ with $t' \in [t_k, t_k + \Delta T]$, a high frequency burst of spikes is then produced (Fig.1B). The proximal and distal bursts can be respectively defined as

$$\begin{aligned} B_i^{t+1} &= \bar{z}_i^t a_i^{t+1} \\ B_i^{*,t+1} &= \bar{z}_i^t a_i^{*,t+1} \end{aligned}$$

This architecture supports a burst-dependent learning rule (Fig.1A, top), enabling target-based learning. More specifically, the pattern of bursts defined by the proximal compartment (receiving the recurrent connections from the network) should mimic the ones defined by the distal compartment (which receives the teaching signal). This is possible by using the following plasticity rule for recurrent weights $J_{ij}^{b \rightarrow p}$ (which can be derived analytically through a likelihood maximization, see methods for details):

$$\Delta J_{ij}^{b \rightarrow p} = \eta \left[a_i^{*,t+1} - a_i^{t+1} \right] \bar{z}_i^t e_j^t \quad (1)$$

where $e_j^t = \partial u_j^t / \partial J_{ij}^{b \rightarrow p}$ is referred to in the literature as the spike response function [Urbanczik and Senn, 2014].

Intuitively, such plasticity rule aims at aligning in time apical proximal spikes with apical distal ones when the somatic window \bar{z}_i^t is open. We remark that such learning rule can be computed online, and requires only observables which are locally accessible to the synapses in space and time.

As a first learning instance, we propose the store-and-recall of a 3D trajectory y_k^{*t} ($k = 1, \dots, 3$, $t = 1, \dots, T$, $T = 1000$) in a network of $N = 500$ neurons (400 excitatory plus 100 inhibitory). We chose y_k^{*t} as a temporal pattern composed of 3 independent continuous signals, each of which specified as the superposition of the four frequencies $f \in \{1, 2, 3, 5\}$ Hz with uniformly extracted random amplitude $A \in [0.5, 2.0]$, and phases $\phi \in [0, 2\pi]$:

$$y_k^{*t} = \sum_{n=1}^4 A_{k,n} \cos(2\pi f_{k,n} t + \phi_{k,n}) \quad , \quad k = 1, 2, 3$$

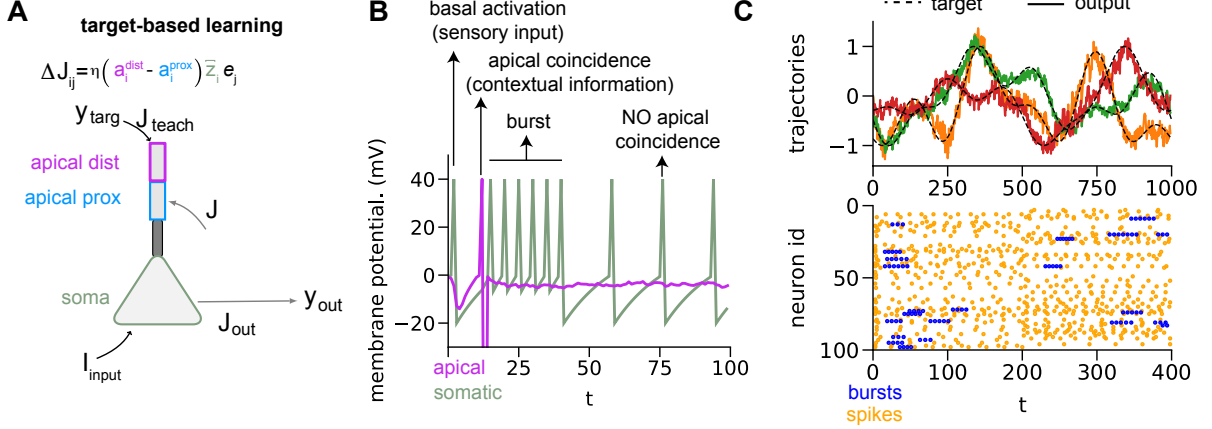


Figure 1: **Model structure A.** The model of a pyramidal neuron, consisting of two separated compartments, the basal and the apical ones. The latter is further divided into two regions, proximal (receiving recurrent connections from the network) and distal (receiving teaching/context signals from other areas of the cortex). **B.** In addition to isolated spike signals emitted by the soma, a coincidence mechanism between basal and apical compartments allows for the generation of high-frequency bursts of spikes. **C.** Store-and-recall of a 3D trajectory. The target output is automatically encoded into a spatio-temporal pattern of bursts (bottom panel), learned online thanks to the plasticity of recurrent connections, allowing for reliable reproduction of the target trajectory (top panel).

This trajectory is randomly projected through a Gaussian matrix with variance σ_{targ}^2 to the apical (distal) dendrites of the network as a teaching signal. This input shapes the spatio-temporal pattern of spikes $a_i^{x,t}$ from the distal apical compartment, as well as the target spatio-temporal pattern of bursts B_i^{*t} (Fig.1C bottom, blue points) as described above.

A clock signal serving as a sensorial input is randomly projected (through a gaussian matrix with variance σ_{in}^2) to the somatic dendrites. In more detail, the clock is here modeled as a sort of time step function with I steps, such that at each time t only component $i = \lfloor I \cdot t/T \rfloor$ is equal to one, while others are zero (see Table.1 for model parameters).

Learning is numerically implemented by several presentations of the same target trajectory y^* to the distal apical compartments, each time adjusting recurrent weights $J_{ij}^{b \rightarrow p}$ according to (1).

Bursting internal activity, which represents the actual quantity mimicking the target, is translated into the output y by means of a read-out matrix J_{out} , randomly initialized and to be trained following the rule derived by minimizing the mean squared error between the target output and the network's output:

$$\Delta J_{ki}^{\text{out}} = \eta_{\text{out}} \left[y_k^{*t} - \sum_h J_{kh}^{\text{out}} \hat{B}_h^t \right] \hat{B}_i^t \quad (2)$$

where \hat{B}_i^t is a time-smoothed version of burst variable

B (see methods for details).

At the end of the learning the plasticity of recurrent connections allows for a reliable reproduction of the target 3D trajectory (see Fig.1C, top, $mse = 0.01$), with an internal bursting activity reproducing the target one (Fig.1C, bottom).

2.2 Apical signals as a flexible context selection

In this section, we show that it is possible to project to the distal apical compartment signal context (through a random matrix with variance σ_{cont}^2) to flexibly select and recall one of the trajectory stored in the network.

In the simplest configuration, two different context binary signals can be projected on the apical compartment, A or B (Fig.2A). In detail, context signal is modeled as a 2D signal, which is $C^t = (1, 0)$ for the context A and $C^t = (0, 1)$ for the context B.

During the training, each context is associated with a well defined target to learn (again a 3D trajectory, as defined in the previous section, Fig.2B, left side, in red and black respectively, only one of the three trajectories is reported for simplicity). To stabilize the learning, we exploited the trick of halving the learning rates η and η_{out} every 100 training iterations. The orthogonality of the contexts and related targets is stressed by imposing a sparsification (of 75% in the

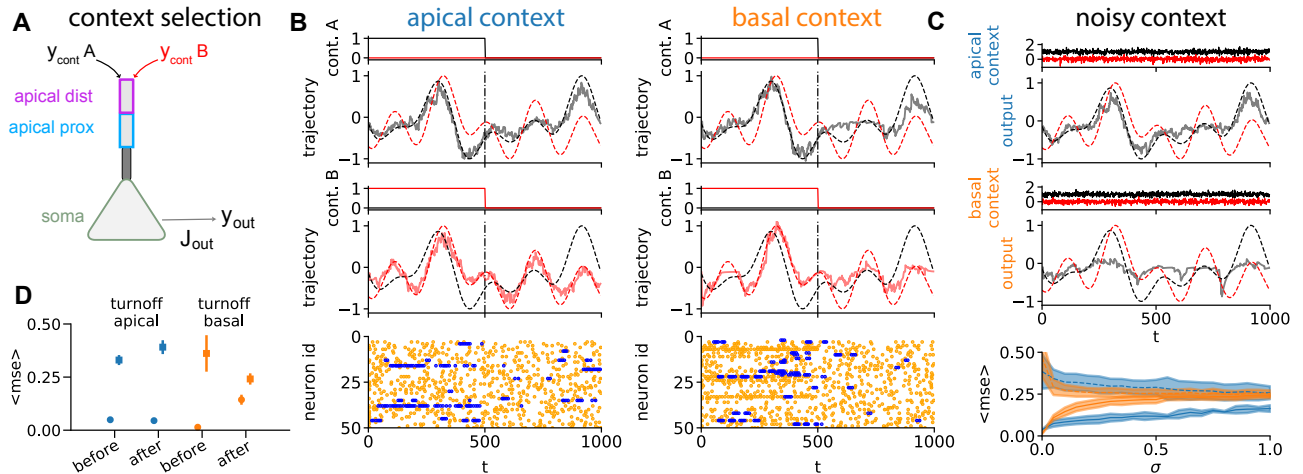


Figure 2: **Apical signals for dynamics selection.** **A.** Model of pyramidal neuron where a binary context signal (A or B) is projected on the apical distal compartment. The target to be reproduced by the network changes according to which context is active. **B.** The network is able to reproduce the correct output trajectory even if the context is provided only in the first time steps. An alternative model in which the context is projected on the basal compartment is no longer able to reproduce the correct output trajectory. **C.** (top) The trajectory produced by the network, in presence of noisy apical context A ($\sigma = 0.2$ black solid line) is similar to the trajectory targeted by the context A (black dashed line) and different from the trajectory targeted by the context B. Inset, the noisy context signal (red dashed line). (middle) The trajectory produced by the network, in presence of noisy basal context A ($\sigma = 0.2$ black line) is NOT similar to the trajectory targeted by the context A (black dashed line). Inset, the noisy context signal. (bottom) The average performances of the apical/basal (blue/orange) context as a function of the noise standard deviation σ . Solid lines: mse between the output and the target output. Dashed lines: mse between the output and the trajectory targeted by the other context. Averages and error bars are intended over many independent network/target realizations. **D.** Summary of performances of the two model versions (context projected on apical vs basal compartment) during “turnoff” test in the middle of the trajectory. Mean square error in the second part of the trajectory (no context) is compared with respect to error in the first part (context still active); mean and variance are intended over many independent network/target realizations.

present case) in the random matrices we use to project the context and the target on the apical compartments of the network.

During the recall phase, the teacher signal is no longer present, while the context signal suggests to the network which of the learned trajectory to reproduce. We show that when the context is projected to the network, the desired output is correctly recalled (Fig.2B, left side). Moreover, if the context signal is turned off in the middle of the trajectory, the network is able to self-sustain its inner dynamics, thanks to recurrent connections (Fig.2B, left side), and correctly replicate the selected trajectory.

The context is here a “suggestion”, so that once started the reproduction of the correct output trajectory, the context itself becomes useless.

To demonstrate the importance to project the context signal in the apical compartments we compare

these results with the case in which the context is projected in the basal ones (both during the training and the retrieval phases).

In this case, the desired trajectory is correctly retrieved when the context is on (Fig.2B, right side).

However, we observe that the basal context is interpreted as a necessary input, so that after the turn-off the network is no longer able to sustain bursts creation, in turn causing a dramatic drop in the test performances (Fig.2B, right side). Average mean square errors, measured against both the correct target trajectory and the wrong one (i.e. the one corresponding to the other context signal), both before turn-off and after it, are provided in Fig.2D for both the neural architectures.

Furthermore, apical context architecture is also robust against corruption in the context signal, which may be the case when at higher cortex level there is

only a mild preference in favor of which strategy to adopt (in comparison with the training phase, where each target is clearly and univocally associated with a sharp context signal). Here a Gaussian white noise of variance σ^2 is added during test to context signals exploited in the training (Fig.2C, top panel, $\sigma = 0.2$). The produced trajectory is similar to the trajectory targeted by the context A (black dashed line) and different from the trajectory targeted by the context B. In Fig.2C, bottom panel (blue lines) it is reported the average *mse* (average over 10 independent realizations of the experiment) between the output and the target trajectory (solid blue line) as a function of σ . As a reference, we also report the *mse* between the output and the trajectory targeted by the other context signal (dashed blue line).

It is evident a resilience of the network with apical context, while the network with basal context suddenly loses the ability to reproduce the desired output already at low levels of noise (Fig.2C, top panel and bottom panel orange lines).

At higher level of noise, basal-context network becomes in practice useless, while apical-context network is still able to reproduce the target trajectory with a remarkably small error (Fig.2C, bottom panel).

2.3 Hierarchical Imitation Learning

The proof that context can be used to flexibly choose which dynamics reproduce (and when), opens the pathway to more complicated neural architectures, naturally supporting hierarchical imitation learning. To our knowledge, no prior works are proposing biologically plausible implementations of hierarchical reinforcement or imitation learning.

We decomposed the network in two sub-networks which we call high-network and low-network (Fig.3A). The high-network (manager) computes the optimal strategy to take to solve a task and sends this information as a context signal to the low-network (worker) which actually executes it.

We applied this strategy to the so-called *button & food* task. In this task, an agent starts at the center of a square domain, which also features a button and an initially locked target (the food). The goal of the agent is to first press the button so to unlock the food and then reach for it. Both button and food positions are uniformly extracted in the domain $[0, 1] \times [0, 1]$. The global task is naturally decomposed into two sub-tasks (or goals): *reach_button* and *reach_food*. The high-network computes which goal to pursue and when, and the low-network implements the sub-policy to achieve the goal.

Both the high- and the low-network share the same input, ($I = 80$ input units) the vertical and horizontal differences of both the button's and food's positions with respect to agent location ($\Delta^t = \{\Delta x_b^t, \Delta y_b^t, \Delta x_f^t, \Delta y_f^t\}$ respectively). These quantities are encoded through a set of tuning curves. Each of the Δ_i values are encoded by 20 input units with different Gaussian activation functions.

To perform learning, we consider a natural hierarchical extension of behavioral cloning. The expert provides a set of hierarchical demonstrations, each consisting of low-level trajectories (to be cloned by the low-network):

$$\{(\text{state}_L^t, \text{action}_L^t, \text{goal}_L^t)\}_{t=1}^T,$$

as well as a high-level trajectory (to be cloned by the high-network):

$$\{(\text{state}_H^t, \text{action}_H^t)\}_{t=1}^T.$$

Both state_L^t and state_H^t are the input Δ^t described above.

The action_H^t is the target output of the high-network and the goal_L^t of the low-network. It is projected to the low-network as a contextual signal in the distal apical compartment (Fig.3B, top) and is defined as a binary two-dimensional teaching signal:

$$\mathbf{y}_H^{*,t} = \chi_{(1)} \Theta(t < t_b) + \chi_{(2)} \Theta(t > t_b),$$

where $\chi_{(i)}$ is one for vector-components i -th and zero otherwise and t_b is the time when the button is reached. Intuitively, this target selects the *reach_button* sub-policy for the first part of the task and then switches to *reach_target*.

Given the input state_L^t and the context goal_L^t , the low-network is tasked to produce as output action_L^t , the velocity vector $\mathbf{y}_L^{*,t} = \mathbf{v}^t = (v_x^t, v_y^t)$, where the velocities are computed so to reach the selected target in a straight line (Fig.3B, center and Fig.3C) and the output is computed as a linear readout of its internal bursting activity (Fig.3B, bottom).

The cloning procedure is implemented as a supervised learning to make the two networks reproduce the target outputs, given the input (and the context). The learning procedure is the same as the one described in Section 2.1. Finally, the two layer network is tested in closed-loop in the environment described above.

The performance in this task is measured via the following quantity:

$$\rho = \frac{\Xi_{\square}}{\min_t d(\mathbf{x}_{\text{agent}}^t, \mathbf{x}_{\text{food}})},$$

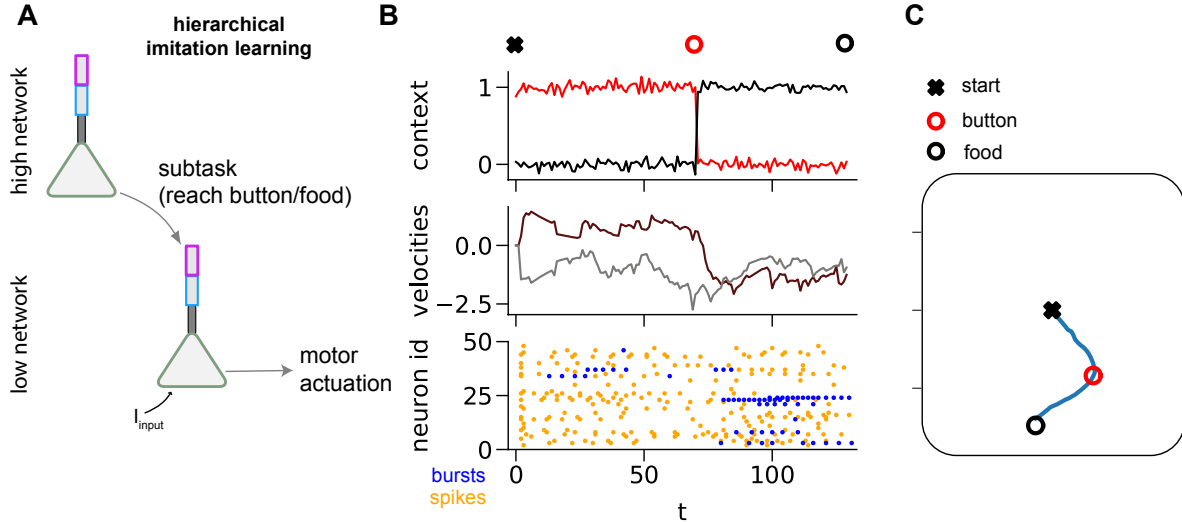


Figure 3: **Hierarchical Imitation Learning** **A**. A two-level network, where high-level neurons produce a signal that serves as a context for the neurons in the low-level network. The two subnetworks received two different but synchronized teaching signals in the training phase. **B**. Button-and-food task, an agent placed at an initial position (black cross) in a 2D maze has to first, reach a button (red circle) and then the food (black circle). The high-level network chooses the order of the subtasks: reach-the-button and then reach-the-food, and projects the instruction as a contextual signal (top panel) to the apical compartments of the low-level network. The low-level network produces the output (velocities of the agent, center panel) necessary to solve the subtask as a readout of its internal bursting activity (bottom panel, blue dots). Orange dots represent the spiking activity. **C**. A sample spatial trajectory. Cross, red and black circles as in panel B.

where Ξ_{\square} is the button-state indicator variable that is zero when the button is locked and one otherwise, the $\mathbf{x}_{(\cdot)}^t$ are the agent and target position vectors and $d(\cdot, \cdot)$ is the standard euclidean distance. The condition for a successful button-press (a switch between locked and unlocked) and target-reach is taken to be $d(\mathbf{x}_{\text{agent}}^t, \mathbf{x}_{\text{btn|food}}) \leq 0.1$. Note how effectively this choice prevents the apparent divergence in the expression for ρ as the episode is stopped when the target is reached, which induces a theoretical maximum achievable score of $\rho_{\max} = 10$.

After the presentation of many randomly positioned button-food pairs, we observe that such two-level network learns to correctly and efficiently solve the button & food task, with an average final score $\rho = 7.3 \pm 4.8$ and over 90% of success rate (i.e. both button-press and target-reach conditions were met). A sample spatial trajectory produced by the network is depicted in Fig.3C.

3 Methods

3.1 The model

Our model of pyramidal neuron considers three different compartments: a basal one (b) and two apical ones, named proximal (p) and distal (d), respectively (see Figure 1 for reference).

Consider a particular neuron i , with $i = 1, \dots, N$, its real vector-valued membrane potential $\mathbf{v}_i^t = (v_i^t, u_i^t, u_i^{*,t})$ (the membrane potentials of the basal, the proximal apical, and distal apical compartments respectively) follows a leaky integrate and fire dynamics, which we can generically write as:

$$\mathbf{v}_i^{t+1} = \left[\left(1 - \frac{dt}{\tau_m} \right) \mathbf{v}_i^t + \frac{dt}{\tau_m} \mathbf{I}_i^{t+1} \right] (1 - \mathbf{s}_i^t) + \mathbf{v}^{\circ} \mathbf{s}_i^t \quad (3)$$

where the vector valued quantities $\mathbf{I}_i^t = (I_{(b),i}^t, I_{(p),i}^t, I_{(d),i}^t)$ $\mathbf{s}_i^t = (z_i^t, a_i^t, a_i^{*,t})$ and $\mathbf{v}^{\circ} = (v_{(b)}^{\circ}, v_{(p)}^{\circ}, v_{(d)}^{\circ})$, respectively the input current, the neuron spike and the reset potential, depend on the compartment (see following sections for explicit definitions). In particular, the neural spike \mathbf{s}_i^t is a stochastic variable determined

via its sigmoidal probability:

$$p(\mathbf{s}_i^{t+1}|\mathbf{v}_i^t) = \frac{\exp\left[\mathbf{s}_i^{t+1}\left(\frac{\mathbf{v}_i^t - v_{\text{thr}}}{\delta v}\right)\right]}{1 + \exp\left(\frac{\mathbf{v}_i^t - v_{\text{thr}}}{\delta v}\right)} \quad (4)$$

with v_{thr} being the firing threshold for the membrane potential and δv a model parameter controlling the probabilistic nature of the neuron. In the $\delta v \rightarrow 0$ limit, the spike-generation rule (4) becomes deterministic:

$$p(\mathbf{s}^{t+1}|\mathbf{v}^t) = \Theta[\mathbf{s}^{t+1}(\mathbf{v}^t - v_{\text{thr}})].$$

We remark that we assume the deterministic limit to numerically implement the dynamics ($\delta v \rightarrow 0$).

3.1.1 Temporal filtering and windows

We introduce the exponential filtering function $\text{filter}(\xi^t, \tau)$, defined recursively as:

$$\begin{aligned} \text{filter}(\xi^{t+1}, \tau) &= \exp\left(-\frac{dt}{\tau}\right) \text{filter}(\xi^t, \tau) + \\ &+ \left(1 - \exp\left(-\frac{dt}{\tau}\right)\right) \xi^{t+1}. \end{aligned} \quad (5)$$

Basal spike signals are time-filtered through suitable time constants, depending on the direction they propagate. Using the previous definition, we introduce the following filtered quantities:

$$\hat{z}_i^{t+1} = \text{filter}(z_i^{t+1}, \tau_s) \quad (6)$$

$$\hat{z}_{\text{ro},i}^{t+1} = \text{filter}(z_i^{t+1}, \tau_{\text{ro}}) \quad (7)$$

$$\hat{z}_{\text{soma},i}^{t+1} = \text{filter}(z_i^{t+1}, \tau_{\text{targ}}) \quad (8)$$

Such filtering is also applied to the adaptatoin term ω_i^t , which is time-smoothed as:

$$\omega_i^{t+1} = \text{filter}(z_i^{t+1}, \tau_\omega). \quad (9)$$

Coincidence between above-threshold somatic spikes $\hat{z}_{\text{soma},i}^t$ and apical proximal a_i^t or apical distal $a_i^{*,t}$ spikes opens a time-window \bar{z}_i^t for bursts onset $\mathbf{B}_i^t = (B_i^t, B_i^{*,t})$:

$$\bar{z}_i^t = \Theta[\hat{z}_{\text{soma},i}^t - \vartheta_{\text{soma}}] \quad (10)$$

The burst variable $\mathbf{B}_i^t \in \{0, 1\} \times \{0, 1\}$ is a tuple of binary variables signaling the onset of a burst activity in the proximal or distal compartments, which can be expressed as:

$$B_i^{t+1} = \bar{z}_i^t a_i^{t+1} \quad (11)$$

$$B_i^{*,t+1} = \bar{z}_i^t a_i^{*,t+1} \quad (12)$$

Aiming for a time-window variable that is active during burst activity, we can iterate the same construction developed for spikes and consider the filtered burst-onset $\hat{\mathbf{B}}_i^t$:

$$\hat{B}_i^{t+1} = \text{filter}(B_i^{t+1}, \tau_{\text{targ}}) \quad (13)$$

$$\hat{B}_i^{*,t+1} = \text{filter}(B_i^{*,t+1}, \tau_{\text{targ}}) \quad (14)$$

One can again use this filtered quantities to introduce proximal and distal burst windows as:

$$\bar{B}_i^{t+1} = \Theta[\hat{B}_i^{t+1} - \vartheta_{\text{burst}}] \quad (15)$$

$$\bar{B}_i^{*,t+1} = \Theta[\hat{B}_i^{*,t+1} - \vartheta_{\text{burst}}] \quad (16)$$

When at least one among proximal and distal bursts is above threshold, we finally have a neural burst activity

$$\bar{B}_{\vee,i}^{t+1} = \bar{B}_i^{t+1} \vee \bar{B}_i^{*,t+1}, \quad (17)$$

which is the quantity that will feature in the dynamics of the compartments.

3.1.2 Basal compartment

The membrane potential of the basal compartment evolves following the equations:

$$\begin{aligned} v_i^{t+1} &= \left[\left(1 - \frac{dt}{\tau_m}\right) v_i^t + \frac{dt}{\tau_m} I_{(b),i}^{t+1} \right] (1 - z_i^t) + \mathbf{v}_{(b)}^\circ z_i^t \\ I_{(b),i}^t &= \sum_{j=1}^N J_{ij}^{b \rightarrow b} z_j^t + \sum_{k=1}^{n_{\text{inp}}} J_{ik}^{\text{inp}} I_k^{\text{inp},t} + \beta \bar{B}_{\vee,i}^t - b \hat{\omega}_i^t + v_0 \end{aligned}$$

With J_{ik}^{inp} and $I_k^{\text{inp},t}$ respectively the input connection matrix and current, while v_0 is a compartment-specific constant input. We introduced the basal reset potential:

$$\mathbf{v}_{(b)}^\circ = \frac{v_{\text{reset},b}}{1 + \alpha \bar{B}_{\vee,i}^t},$$

Where $v_{\text{reset},b}$ is a compartment-specific scalar, α is a constant model parameter and $\bar{B}_{\vee,i}^t$ is the active burst-window variable (see section TEMPORAL FILTERING AND WINDOWS for and explicit characterization). Note how during the burst-window $\bar{B}_{\vee,i}^t$ the soma receives an extra input and the reset potential is higher, we set $\alpha = 2$ and $\beta = 20$ to define the entity of such effects.

3.1.3 Apical proximal compartment

The apical proximal compartment of each neuron is connected to basal compartments of all the neurons through recurrent connections $J_{ij}^{b \rightarrow p}$ (the ones to be

trained to reproduce the desired target). The equation for this compartment’s dynamics are:

$$u_i^{t+1} = \left[\left(1 - \frac{dt}{\tau_m} \right) u_i^t + \frac{dt}{\tau_m} I_{(p),i}^{t+1} \right] (1 - a_i^t) + v_{(p)}^\circ a_i^t$$

$$I_{(p),i}^t = \underbrace{\sum_{j=1}^N J_{ij}^{b \rightarrow p} \hat{z}_j^t(t)}_{\text{recurrent basal-proximal connections}} + u_0$$

The reset potential for the proximal apical compartment $v_{(p)}^\circ = v_{\text{reset},p}$ is a compartment-specific scalar, independent of burst activity, while u_0 is the compartment constant input.

3.1.4 Apical distal compartment

The signal to be learned (target) is considered as an input for the apical distal compartment: coefficient f_{apic} is set to 1 during the learning stage, and then set to 0 to get rid of this term during spontaneous activity. Also, the input from the context (again randomly projected on the N neurons) is given as input for the apical distal compartment. The equations for the apical distal compartment read:

$$u_i^{*,t+1} = \left[\left(1 - \frac{dt}{\tau_m} \right) u_i^{*,t} + \frac{dt}{\tau_m} I_{(d),i}^{t+1} \right] (1 - a_i^{*,t}) + v_{(d)}^\circ a_i^{*,t}$$

$$I_{(d),i}^t = f_{\text{apic}} \underbrace{\sum_{k=1}^{n_{\text{output}}} J_{ik}^{\text{target}} y_k^{*,t}}_{\text{target/teach input}} + \underbrace{\sum_{k=1}^{n_{\text{cont}}} J_{ik}^{\text{cont}} C_k^t}_{\text{context}} + u_0^*$$

where $y_k^{*,t}$ is the target signal and C_k^t the context signal, while u_0^* is the compartment constant input. We report the model parameters, for the three figures, in Table.1.

3.2 Derivation of the learning rule

We derive the update rule for the recurrent weights of the network by maximizing the probability to reproduce the target spatio-temporal pattern of bursts, extending previous approaches used for learning target pattern of spikes [Pfister et al., 2006, Jimenez Rezende and Gerstner, 2014, Gardner and Grüning, 2016, Muratore et al., 2021]. The first step is to write the probability to produce a burst in the neuron i at time t , given the somatic window \bar{z}_i^t . We propose the following compact formulation:

$$p(B_i^{*,t+1} | \bar{z}_i^t) = \frac{\exp \left[B_i^{*,t+1} \Phi_i^t(\bar{z}_i^t) \right]}{1 + \exp \left[\Phi_i^t(\bar{z}_i^t) \right]} \quad (18)$$

Table 1: **Parameter of numerical simulations.**

Many parameters have the same value for all the simulations reported in the main text figures. When not the case, the different values used are clearly indicated. For FIG 3 two values for low network (L) and high network (H), respectively, have been reported, when different from each other. For FIG 2 η and η_{out} we report the initial parameter values, during learning they are discounted as discussed in section 2.2.

| PARAMETER | FIG 1 | FIG 2 | FIG 3 [L-H] |
|----------------------------|-------|-----------------------|-------------|
| N | 500 | 1000 | 500-500 |
| σ_{targ} | 20 | 30 | 0-100 |
| σ_{in} | 12 | 12 | 20 |
| η | 10 | 10 | 0-0.25 |
| η_{out} | 0.01 | 0.01 | 0.03 |
| I | 5 | 50 | N.D. |
| σ_{cont} | 0 | 20 | 50-0 |
| N_e | | 80% N | |
| N_i | | 20% N | |
| τ_m | | 20 (ms) | |
| τ_s | | 2 (ms) | |
| τ_{out} | | 10 (ms) | |
| τ_{targ} | | 20 (ms) | |
| τ_ω | | 200 (ms) | |
| b | | 100 | |
| $v_{\text{reset},b}$ | | -20 (mV) | |
| $v_{\text{reset},d,p}$ | | -160 (mV) | |
| v_0 | | -1 (mV) | |
| u_0 | | -6 (mV) | |
| u_0^* | | -6 (mV) | |
| v_{thr} | | 0 (mV) | |
| ϑ_{soma} | | 2.5×10^{-2} | |
| ϑ_{burst} | | 1.25×10^{-2} | |

where we have introduced $\Phi_i^t(\bar{z}_i^t) = a_i^t \bar{z}_i^t / \delta v - (1 - \bar{z}_i^t) \gamma$. By definition, a burst can only happen by means of a basal-apical spike coincidence, represented by the $a_i^t \bar{z}_i^t$ term. When the basal window is open ($\bar{z}_i^t = 1$) the burst probability reduces to the usual sigmoidal function. When the window is closed and $\bar{z}_i^t = 0$, we have $\Phi_i^t(\bar{z}_i^t) = -\gamma$, we can thus tune the γ parameter to model the burst probability. In practice, we work in the $\gamma \rightarrow \infty$ limit where $\lim_{\gamma \rightarrow \infty} p(B_i^{*,t+1} | \bar{z}_i^t = 0) = 0$, which agrees to the intuitive understanding that a closed basal window prevents any burst activity. We introduce the likelihood \mathcal{L} of observing a given target burst activity \mathbf{B}^* given the basal-to-proximal

connections $J_{ij}^{b \rightarrow p}$ as:

$$\mathcal{L}(\mathbf{B}^* | J^{b \rightarrow p}) = \sum_{it} \left[B_i^{*,t+1} \Phi_i^t(\bar{z}_i^t) + \right. \\ \left. - \log(1 + \exp[\Phi_i^t(\bar{z}_i^t)]) \right] \quad (19)$$

We can then maximize this likelihood by adjusting the synaptic connection so to achieve the target burst activity \mathbf{B}^* . By differentiating with respect to the recurrent apical weights, we get:

$$\frac{\partial \mathcal{L}(\mathbf{B}^* | J^{b \rightarrow p})}{\partial J_{ij}^{b \rightarrow p}} = \left[B_i^{*,t+1} - p(B_i^{t+1} = 1) \right] \bar{z}_i^t e_j^t \quad (20)$$

where we have introduced the following two quantities:

$$p(B_i^{t+1} = 1) = \frac{\exp[\Phi_i^t(\bar{z}_i^t)]}{1 + \exp[\Phi_i^t(\bar{z}_i^t)]} \quad \text{and} \quad e_j^t = \frac{\partial u_i^t}{\partial J_{ij}^{b \rightarrow p}}.$$

Given the basal window \bar{z}_i^t state, the target burst sequence is uniquely defined by the input projected to the apical distal compartment and can be written as $B_i^{*,t+1} = \bar{z}_i^t a_i^{*,t+1}$. If we take the model deterministic limit ($\delta v \rightarrow 0$, where $p(B_i^{t+1} = 1) = a_i^{t+1} \bar{z}_i^t$) and note that $\bar{z}_i^t \bar{z}_i^t = \bar{z}_i^t$, we can rewrite the previous expression in a cleaner form:

$$\frac{\partial \mathcal{L}(\mathbf{B}^* | J^{b \rightarrow p})}{\partial J_{ij}^{b \rightarrow p}} = \left[a_i^{*,t+1} - a_i^{t+1} \right] \bar{z}_i^t e_j^t. \quad (21)$$

This means that the spikes in the proximal apical compartment a_i^{t+1} should mimic the ones in the distal one $a_i^{*,t+1}$, when the somatic window \bar{z}_i^t is open. For simplicity, we discussed this version of the learning rule. However, in this work we used the non-deterministic version of the rule (finite $\delta v = 0.1$) that can be rewritten as:

$$\frac{\partial \mathcal{L}(\mathbf{B}^* | J^{b \rightarrow p})}{\partial J_{ij}^{b \rightarrow p}} = \left[a_i^{*,t+1} - p(a_i^{t+1} = 1 | u_i^t) \right] \bar{z}_i^t e_j^t. \quad (22)$$

where $p(a_i^{t+1} = 1 | u_i^t) = \frac{\exp\left(\frac{u_i^t - v_{\text{thr}}}{\delta v}\right)}{1 + \exp\left(\frac{u_i^t - v_{\text{thr}}}{\delta v}\right)}$. We stress

here how in the derivation we considered the basal-window state \bar{z}_i^t as given. Consequently, the target burst sequence \mathbf{B}^* is uniquely defined by the input projected to the apical distal compartment and the likelihood is well defined. We are aware however of the feedback influence of the burst activity on the basal-window configuration (bursts induce basal spikes, see the equation for basal current $I_{(b),i}^t$ in the BASAL COMPARTMENT section), we chose to neglect such contribution as it would have severely increased the difficulty

of the derivation. The convergence to the chosen target thus cannot be granted. Despite the fact that we cannot theoretically prove the convergence of the learning rule, we provide a numerical demonstration that the target pattern of bursts converges to a well defined pattern (see Appendix for details).

3.3 Source code availability

The source code is available for download under CC-BY license in the

<https://github.com/cristianocapone/LTTB> public repository.

4 Discussion

In the present work, we have shown that the anatomy of pyramidal neuron can naturally support target-based learning. Moreover, it allows for using contextual signals to flexibly select the desired output from a repertoire of learned dynamics.

These properties naturally combine together to orchestrate a network with a hierarchical architecture, which in turn lends itself to *hierarchical imitation learning* (HIL) [Le et al., 2018]. HIL enables the decomposition of challenging long-horizon decision-making tasks into simpler sub-tasks, improving both learning speed and transfer learning, as skills learned by sub-modules can be re-used for different tasks. In our work, a high-level network (the manager) selects the correct policy for the task, while the low-level network (the worker) is in charge of actually executing it.

To our knowledge, there exist no other works proposing a biologically plausible architecture to implement HIL. Furthermore, our model prepares the ground for further biological explorations. Model parameters (e.g., the adaptation strength b) allows simulating the transition between different brain states (e.g., sleep and awake) [Wei et al., 2018, Goldman et al., 2020, Tort-Colet et al., 2021]. Possible future investigation topics include replay of the pattern of bursts during sleep [Kaefer et al., 2020], and the effect of sleep on tasks performances [Wei et al., 2018, Capone et al., 2019].

Acknowledgement

This work has been supported by the European Union Horizon 2020 Research and Innovation program under the FET Flagship Human Brain Project (grant agreement SGA3 n. 945539 and grant agreement SGA2 n.

785907) and by the INFN APE Parallel/Distributed Computing laboratory.

References

- [Bellec et al., 2020] Bellec, G., Scherr, F., Subramoney, A., Hajek, E., Salaj, D., Legenstein, R., and Maass, W. (2020). A solution to the learning dilemma for recurrent networks of spiking neurons. *Nature communications*, 11(1):1–15.
- [Capone et al., 2021] Capone, C., Muratore, P., and Paolucci, P. S. (2021). Error-based or target-based? a unifying framework for learning in recurrent spiking networks. *arXiv preprint arXiv:2109.01039*.
- [Capone et al., 2019] Capone, C., Pastorelli, E., Golosio, B., and Paolucci, P. S. (2019). Sleep-like slow oscillations improve visual classification through synaptic homeostasis and memory association in a thalamo-cortical model. *Scientific reports*, 9(1):1–11.
- [DePasquale et al., 2018] DePasquale, B., Cueva, C. J., Rajan, K., Escola, G. S., and Abbott, L. (2018). full-force: A target-based method for training recurrent networks. *PloS one*, 13(2):e0191527.
- [Gardner and Grüning, 2016] Gardner, B. and Grüning, A. (2016). Supervised learning in spiking neural networks for precise temporal encoding. *PloS one*, 11(8):e0161335.
- [Goldman et al., 2020] Goldman, J., Kusch, L., Hazalyalcinkaya, B., Depannemaeker, D., Nghiem, T.-A., Jirsa, V., and Destexhe, A. (2020). Brain-scale emergence of slow-wave synchrony and highly responsive asynchronous states based on biologically realistic population models simulated in the virtual brain. *BioRxiv*.
- [Guerguiev et al., 2017] Guerguiev, J., Lillicrap, T. P., and Richards, B. A. (2017). Towards deep learning with segregated dendrites. *Elife*, 6:e22901.
- [Jimenez Rezende and Gerstner, 2014] Jimenez Rezende, D. and Gerstner, W. (2014). Stochastic variational learning in recurrent spiking networks. *Frontiers in Computational Neuroscience*, 8:38.
- [Kaefer et al., 2020] Kaefer, K., Nardin, M., Blahna, K., and Csicsvari, J. (2020). Replay of behavioral sequences in the medial prefrontal cortex during rule switching. *Neuron*, 106(1):154–165.
- [Larkum, 2013] Larkum, M. (2013). A cellular mechanism for cortical associations: an organizing principle for the cerebral cortex. *Trends in neurosciences*, 36(3):141–151.
- [Le et al., 2018] Le, H., Jiang, N., Agarwal, A., Dudik, M., Yue, Y., and Daumé III, H. (2018). Hierarchical imitation and reinforcement learning. In *International conference on machine learning*, pages 2917–2926. PMLR.
- [Lee et al., 2015] Lee, D.-H., Zhang, S., Fischer, A., and Bengio, Y. (2015). Difference target propagation. In *Joint european conference on machine learning and knowledge discovery in databases*, pages 498–515. Springer.
- [Manchev and Spratling, 2020] Manchev, N. and Spratling, M. W. (2020). Target propagation in recurrent neural networks. *J. Mach. Learn. Res.*, 21:7–1.
- [Meulemans et al., 2020] Meulemans, A., Carzaniga, F. S., Suykens, J. A., Sacramento, J., and Grewe, B. F. (2020). A theoretical framework for target propagation. *arXiv preprint arXiv:2006.14331*.
- [Muratore et al., 2021] Muratore, P., Capone, C., and Paolucci, P. S. (2021). Target spike patterns enable efficient and biologically plausible learning for complex temporal tasks. *PloS one*, 16(2):e0247014.
- [Nicola and Clopath, 2017] Nicola, W. and Clopath, C. (2017). Supervised learning in spiking neural networks with force training. *Nature communications*, 8(1):2208.
- [Pateria et al., 2021] Pateria, S., Subagdja, B., Tan, A.-h., and Quek, C. (2021). Hierarchical reinforcement learning: A comprehensive survey. *ACM Computing Surveys (CSUR)*, 54(5):1–35.
- [Payeur et al., 2021] Payeur, A., Guerguiev, J., Zenke, F., Richards, B. A., and Naud, R. (2021). Burst-dependent synaptic plasticity can coordinate learning in hierarchical circuits. *Nature neuroscience*, pages 1–10.
- [Pfister et al., 2006] Pfister, J.-P., Toyoizumi, T., Barber, D., and Gerstner, W. (2006). Optimal spike-timing-dependent plasticity for precise action potential firing in supervised learning. *Neural computation*, 18(6):1318–1348.
- [Poirazi and Papoutsi, 2020] Poirazi, P. and Papoutsi, A. (2020). Illuminating dendritic function with computational models. *Nature Reviews Neuroscience*, 21(6):303–321.

- [Sacramento et al., 2018] Sacramento, J. a., Ponte Costa, R., Bengio, Y., and Senn, W. (2018). Dendritic cortical microcircuits approximate the backpropagation algorithm. In Bengio, S., Wallach, H., Larochelle, H., Grauman, K., Cesa-Bianchi, N., and Garnett, R., editors, *Advances in Neural Information Processing Systems 31*, pages 8721–8732. Curran Associates, Inc.
- [Tort-Colet et al., 2021] Tort-Colet, N., Capone, C., Sanchez-Vives, M. V., and Mattia, M. (2021). Attractor competition enriches cortical dynamics during awakening from anesthesia. *Cell Reports*, 35(12):109270.
- [Urbanczik and Senn, 2014] Urbanczik, R. and Senn, W. (2014). Learning by the dendritic prediction of somatic spiking. *Neuron*, 81(3):521–528.
- [Wei et al., 2018] Wei, Y., Krishnan, G. P., Komarov, M., and Bazhenov, M. (2018). Differential roles of sleep spindles and sleep slow oscillations in memory consolidation. *PLoS computational biology*, 14(7):e1006322.

Appendix: Burst-dependent plasticity and dendritic amplification support target-based learning and hierarchical imitation learning

A Numerical evidence of convergence

As mentioned above, we can not provide a mathematical proof of the convergence toward the chosen target of burst activity by means of the learning rule proposed here. However, strong evidences in this direction can be found numerically.

We run several independent realizations of the same task of Fig.1, i.e., the store-and-recall of a 3D trajectory. We look at the distance between the target and the spontaneous spatio-temporal pattern of bursts during the training, and also at the self-distance in the pattern of spontaneous bursts across consecutive training iterations.

The parameters used for these simulations (when different from those used for Fig.1) are: $\eta = 2.5$, $\eta_{\text{out}} = 2.5 \times 10^{-3}$, σ_{targ} variable from 10 (black) to 1000 (yellow). Data averaged over 10 independent network/target realizations. The distance between two patterns of bursts $A = \{A_i^t\}$ and $B = \{B_i^t\}$ is defined as:

$$\mathcal{D}(A, B) \equiv \sqrt{\frac{1}{NT} \sum_{i=1}^N \sum_{t=1}^T (A_i^t - B_i^t)^2}$$

For small values of σ_{targ} , comparable to the ones used for main text figures, target bursts rapidly settle after some hundreds of training iterations (Fig.4A); within the same training scale, also spontaneous burst activity matches the target one, with a negligible error (Fig.4B). Accordingly, the overall number of bursts is the same for target and spontaneous activity (Fig.4C).

We prove that in a broad range of σ_{targ} values, the target pattern of bursts converges to a well defined one ((Fig.4C blue dots), up to $\sigma_{\text{targ}} = 100$) even though the number of bursts increases for high values of σ_{targ} (Fig.4C red dots).

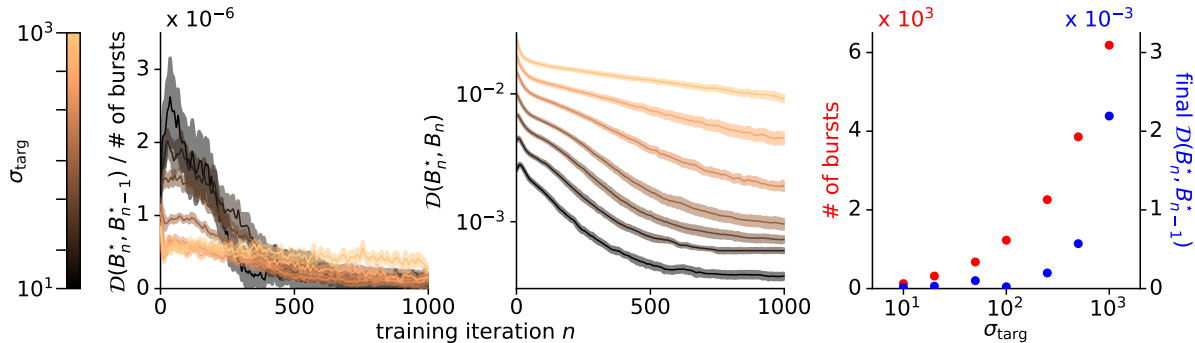


Figure 4: **Convergence of the target pattern of bursts.** (left) $\mathcal{D}(B_n^*, B_{n-1}^*) / (\text{number of bursts})$ as a function of the number n of learning iterations, for different σ_{targ} values (lower to higher values, from dark to light). (middle) Distance between the target and spontaneous pattern of bursts $\mathcal{D}(B_n^*, B_n)$ after n learning iterations. (right) Blue: average final $\mathcal{D}(B_n^*, B_{n-1}^*) / (\text{number of bursts})$ value as a function of σ_{targ} . Red: average number of bursts as a function of σ_{targ} .